

Interference effects of three consecutive wall-mounted cubes placed in deep turbulent boundary layer

Hee Chang Lim^{1,†} and Masaaki Ohba²

¹School of Mechanical Engineering, Pusan National University, 2, Busandaehak-ro 63beon-gil, Geumjeong-gu, Busan 609-735, South Korea

²Department of Architecture, Faculty of Engineering, Tokyo Institute of Polytechnics, Atsugi, Kanagawa 243-02/3, Japan

(Received 12 July 2013; revised 11 May 2014; accepted 1 August 2014;
first published online 1 September 2014)

In this study we undertook various calculations of the turbulent flow around a building in close proximity to neighbouring obstacles, with the aim of gaining an understanding of the velocity and the surface-pressure variations with respect to the azimuth angle of wind direction and the gap distance between the obstacles. This paper presents the effects of flow interference among consecutive cubes for azimuth angles of $\theta = 0, 15, 30,$ and 45° and gap distances of $G = 0.5h, 1.0h, 1.5h,$ and ∞ (i.e. a single cube), where h is the cube height, placed in a turbulent boundary layer. A transient detached eddy simulation (DES) was carried out to calculate the highly complicated flow domain around the three wall-mounted cubes to observe the fluctuating pressure, which substantially contributes to the suction pressure when there is separation and reattachment around the leading and trailing edges of the cubes. In addition, the results indicate that an increasing azimuth angle increases the pressure variation on the centre cube of the three parallel-aligned cubes. The mean pressure variation can even change from negative to positive on the side face. Owing to interference effects, the mean pressure coefficient of the centre cube of the three parallel-aligned cubes was generally lower than the coefficient of the single cube and tended to increase depending on the gap distance. Furthermore, when the three consecutive cubes are in a tandem arrangement, the gap distance has little influence on the first cube but results in significant interference effects on the second and third cubes.

Key words: flow-structure interactions, separated flows, turbulent boundary layers

1. Introduction

Over the past several decades, the wind load characteristics around bluff bodies have been of fundamental interest in the study of fluid dynamics, which has long been considered a critical design parameter for various engineering disciplines: civil, fluid mechanical and architectural. Regarding a simple cubic bodies, numerous empirical and simulated data and comparisons of the flow around the body have been carried

[†] Email address for correspondence: hclim@pusan.ac.kr

out (e.g. Castro & Robins 1977 (hereafter, CR); Tieleman & Akins 1996; Richards, Hoxey & Short 2001 (hereafter, RHS); Lim, Castro & Hoxey 2007 (hereafter, LCH); Lim, Thomas & Castro 2009 (hereafter, LTC)). However, in terms of practical applicability, such as a group of structures or an occupied solidity of distributed houses and buildings, the single bluff body is not appropriate. Therefore, studies have shifted toward the arrangement and the configuration of a group of building structures (e.g. Zdravkovich 1977; Khanduri, Stathopoulos & Bedard 1998; Xie & Gu 2004; Xie & Gu 2007; Kim, Tamura & Yoshida 2011). Most of the previous studies fall into one of three categories: tandem arrangements, in which one building is directly in the wake of the other; side-by-side arrangements, in which buildings are arranged transverse to the incoming flow; and staggered arrangements, in which buildings are arbitrarily configured (Khanduri *et al.* 1998). The flow field, pressure coefficients, force variation, and amplification or suppression of vortex shedding are highly dependent on the configuration of the building and on the shape and spacing of the building group because of both the wake- and proximity-induced interference effects.

Regarding the flow around cylindrical models of consecutive bodies, Zdravkovich (1977, 1987) are frequently cited because they describe wind-tunnel experiments that measured the flow around two surface-mounted cylinders. In these papers, Zdravkovich analysed the problem of flow interference that arises when two cylinders are placed side-by-side, in tandem, and in staggered arrangements under steady-state conditions. He observed that the vortex-induced force and the vortex shedding pattern were considerably different from those calculated for a single cube of the same Reynolds number. This was one of the first demonstrations of the crucial importance of the appropriate modelling of the design details of a building configuration. However, this early work only focused on the appropriate simulation of the building arrangements. Following Zdravkovich's study, many other studies examined the interference phenomenon for two-dimensional (2D) and three-dimensional (3D) bodies. The 2D obstacles with a sufficient span for eliminating the end effects are traditionally modelled as long-span pipes or cylinders immersed in a uniform oncoming stream. Most of the previous research on 2D geometries concentrated on circular cylinders (e.g. Bearman & Wadcock 1973; Zdravkovich 1977; Sumner, Price & Paidoussis 1999; Sumner, Richards & Akosile 2005; Kitagawa & Ohta 2008). Bearman & Wadcock (1973), for example, investigated the effect of interference on two 2D cylinders in a side-by-side arrangement. They measured the pressure distribution around the bodies and determined there is a repulsive force between the cylinders for a particular range of gaps. For a small gap, they observed a marked asymmetry in the flow and different drag and base pressure coefficients for each of the two cylinders.

Structures with circular cross-sections experience flow-induced instabilities; structures with fixed flow-separation positions, such as cylinders with square or rectangular cross-sections, also experience 3D flow instabilities. As an example, 2D tandem and side-by-side arrangements of two square cylinders represent idealizations of the flow interference that occurs in an array of cylinders. Previous studies have established the mean characteristics of the flow and the mean pressure loading, depending on the bluff-body arrangement. Unsteady phenomena are not studied extensively, particularly in the case of more complex configurations. Nevertheless, the vorticity structure and the oscillating velocity components present in the flow accompanied by periodic events, such as vortex shedding, vortex resonance and galloping, are the major causes of flow-induced instabilities around square or rectangular cylinders, which complicates further studies (Zdravkovich 1977).

The 3D rectangular and square-sectional models have not been studied expansively. The 3D configuration includes all cases for which the end effects are significant (Sakamoto & Haniu 1988; Martinuzzi & Havel 2000). Owing to their practical relevance, this study focused on wall-mounted geometries. These flows differ from those in the 2D cases because of the advection of the upstream vorticity in the oncoming boundary layer and the existence of mean streamwise vortices, which strongly influence the momentum transfer normal to the main stream. The evolution of the wakes formed behind a pair of cylinders placed side-by-side was also studied by Williamson (1985). The paper presented that the wakes were synchronized either in phase or in antiphase for a certain range of gaps between the cylinders. When the gap between the cylinders decreased below the critical minimum gap, the flow became asymmetric, which is similar to the result obtained by Bearman & Wadcock (1973). Other noteworthy experimental studies are published in Arie *et al.* (1983), Kim & Durbin (1988) and Sumner, Price & Paidoussis (1998).

A number of findings regarding flow interference were obtained; most of the studies involved only two bodies in close proximity (Kim *et al.* 2011). The most common interference mechanisms include the shelter effect, flow channeling, flow asymmetry and wake buffeting. When two buildings are in a tandem arrangement, the upstream building generally provides shielding for the downstream building. This normally leads to a reduction in the mean in-line force on the downstream building. However, fluctuating wind forces can increase because of turbulence buffeting (Bailey & Kwok 1985). The presence of a neighbouring building introduces asymmetry in the wind flow pattern around the target building, leading to the possibility of highly magnified, wind-induced torsion (Zhang & Kwok 1994). The upstream building is not significantly affected by a downstream building, but when two buildings are in close proximity, the wind flow is channeled to sweep through the building gap.

Above all, research on two bluff bodies placed close together is considered to be important owing to their mutual interaction effects. Ricciardelli & Vickery (1998) investigated the aerodynamic forces acting on a pair of square cylinders in both tandem and side-by-side arrangements. They measured the pressure in smooth and turbulent flows with azimuth angles (e.g. 0° is defined as the angle of normal incidence on the model) ranging from 0 to 90° and wide-range separations from $2h$ to $13h$, where h is the model height. They observed that for large angles of flow incidence, as the gap increased, the values of the root-mean-square (r.m.s.) force coefficients increased. In addition, To & Lam (2003) reported some interference effects not previously observed in past investigations on two buildings and a group comprising three or more buildings. However, interference effects on a group of three or more buildings have not been studied in detail thus far, and many problems still must be investigated Xie & Gu (2004, 2007).

This paper emphasizes the characteristics of a group of cubic bodies with various gaps. The gap between the bodies is responsible for the type of wakes generated behind and between bodies and, ultimately, for the structural loading, pressure and, in particular, structural excitation. For example, with the inclusion of another building in a side-by-side arrangement, the loading pattern becomes quite complex. The buildings may experience increased or reduced wind loads depending on their geometries and spacing, as well as the characteristics of the wind flow and the upstream terrain. Regarding the gap distance, Tang & Kwok (2004) observed the interference effect of two CAARC (Commonwealth Advisory Aeronautical Research Council) building models in a boundary layer wind tunnel. Their goal was to determine the interference between buildings, where one of the buildings was located far upstream or downstream

(approximately $2B$ – $10B$) of the principal building. Similarly, Thepmongkorn, Wood & Kwok (2002) also reported the interference effects on wind-induced coupled translation-torsional motion, with building spacing ranging from $3B$ to $8B$, where B was the depth of the building. Kim *et al.* (2011) examined the interference factors (IFs) of two tall buildings in order to determine the maximum positive and minimum negative peak pressures of the principal building for a variety of locations of the interfering building (e.g. $1.5B$ – $8.5B$). In addition, Hui, Tamura & Yoshida (2012), Hui, Yoshida & Tamura (2013) investigated the interference effects between two rectangular-section buildings, focusing on the local peak pressure for various configurations with building spacing ranging from $1.5B$ to $7B$. Recently, Thool, Ashok & Anupam (2013) attempted to study the effect of a small building on wind loads acting on a comparatively larger building for a wide range of spacings from $0.25B$ to $20B$. In these study, they targeted the flow-induced load properties of real towers or buildings in an urban area so that the response characteristics are closer to the requirements of the engineering field, although the characteristics can be somewhat out of range for the purpose of fluid mechanics.

This paper consists of a set of simulations on the boundary layer flow for different azimuth angles around three surface-mounted cubes that in both parallel-aligned and tandem arrangements. Here, the emphasis is on the effect of the azimuth angle of the incident flow (i.e. 0 , 15 , 30 and 45°) and the gap distance between the cubes (i.e. $G = 0.5h$, $1.0h$, $1.5h$ and ∞ (i.e. a single cube), where h is the cube height). There are numerous key points here. We summarize our major findings as follows. (i) For flows and wind loads around multiple obstacles, the gap distance and azimuth angle are significantly important and can be used for the design of the deployment and arrangement of neighbouring buildings and structures. (ii) Despite the lack of wind tunnel data, there are new mean flow data, as well as fluctuating quantities, for the single- and triple-cube cases. In addition, (iii) this paper includes much more reasonable and improved mean and turbulence quantities, as well as the interference effect of multiple obstacles according to the detached eddy simulation (DES) calculation. (iv) We observed that the peak fluctuating pressure and gap distance have a substantial effect on the central cube of the three parallel-aligned cubes but not on a single cube; this phenomenon had never been achieved before.

This paper is systematically organized as follows. Section 2 details the computational techniques, including the set-up of the computational wind tunnel, the selection of the turbulence model, and the generation of the turbulent boundary layer. Section 3 presents the results and analysis. More specifically, § 3.1 describes the surface pressure variation around a single cube, which enables a comparison against previous studies. Sections 3.2 and 3.3 describe the interference effects of the azimuth angle and the gap distance resulting from the three parallel-aligned cubes, respectively. Section 3.4 describes the gap distance effect resulting from the three tandem cubes. Finally, § 4 outlines the major conclusions.

2. Computational techniques

2.1. Numerical methods

Figure 1 shows the schematic diagram of the numerical domain for a single cube, three parallel-aligned cubes and three tandem cubes. The entire domain containing the cube models, internal working section and surface wall as well as the boundary conditions (e.g. inlet, symmetry, periodicity, outlet, wall conditions, etc.) are shown in each figure. The symbol G in figure 1(b and c) denotes the gap distance between the

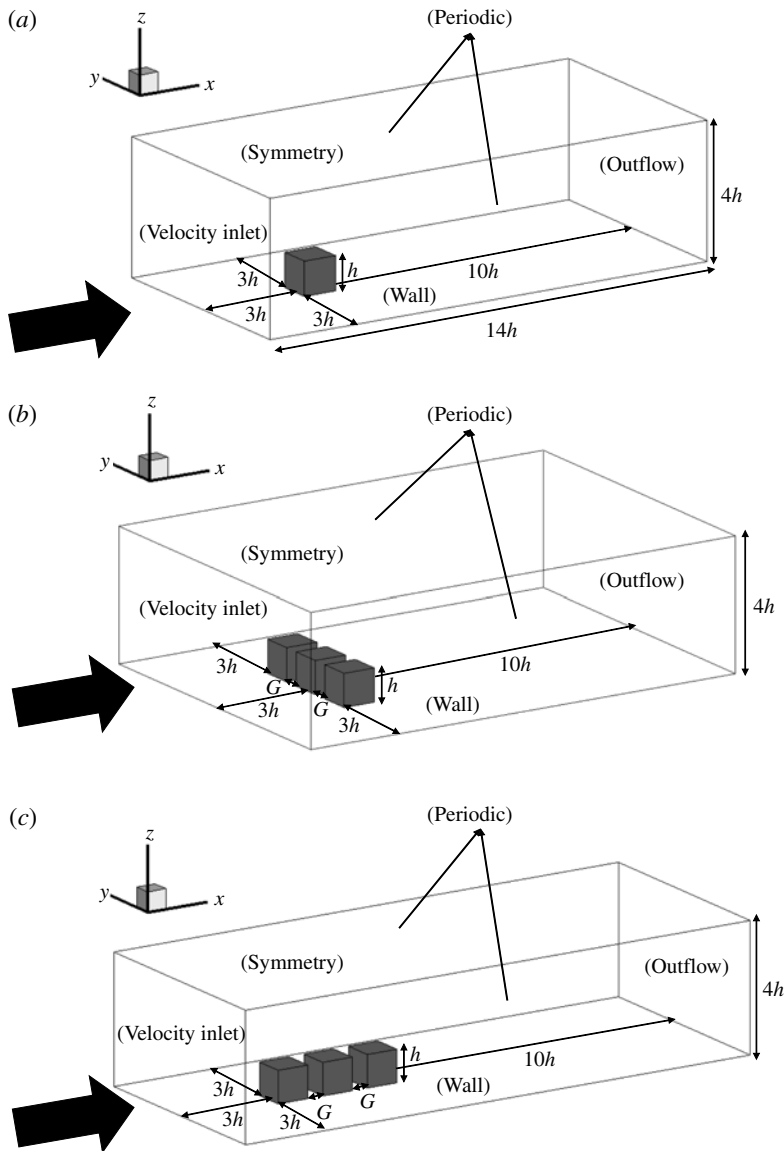


FIGURE 1. Schematic diagram of the cube models and the domain used for the numerical tunnel: (a) a single cube; (b) three parallel-aligned cubes; and (c) three tandem cubes.

consecutive cubes. In this study, the values of the gap G were $0.5h$, $1.0h$, $1.5h$ and ∞ (i.e. a single cube), where h represents the cube height (i.e. 150 mm). When the gap distance changed, the entire domain, including the size and the number of mesh grids, was regenerated to produce small-scale turbulence. To ensure the feasibility of the numerical domain, the cubes were placed $3h$ downstream from the inlet domain and $10h$ upstream from the outlet. In addition, the distance between the side and roof surfaces and the far outer boundary surface was at least $3h$.

In order to resolve the small-scale turbulent flow, computational meshes were carefully designed to be dense on the wall surface and to be coarse in the far-field to

obtain an appropriate solution for the DES. Therefore, the first grid spacing near the wall was at $0.025h$, and the spacing ratio was 1.1 in order to ensure that the value of y^+ (e.g. $y^+ = 35$) for the wall was acceptable, as suggested by Salim & Cheah (2009). In addition, when the aspect ratio of the model changed in this study, the entire domain, including the mesh grid and model size, needed to be reconstructed, as shown in figure 1. The entire domains containing the cube models, internal working section and surface wall are shown in each figure, along with the boundary conditions for the flow. Five different boundary conditions were used in the numerical domain: the inlet and outlet flow conditions for the inlet/outlet domain, periodicity for the side, symmetry for the upper wall, and wall conditions for the rest of the surface wall. In this study, the mesh was made using ICEM CFD 14.0, and the DES turbulence model was selected to calculate these cases. The solver was designed for a pressure-based, incompressible flow. Standard wall functions, which are provided as a default option in ANSYS FLUENT[®], were applied. Furthermore, for the spatial discretisation solution methods, we selected the least-squares cell-based method for the gradient, standard method for the pressure, bounded central differencing method for the momentum and second-order upwind method for the modified turbulent viscosity. A 3D turbulence model of the problem was formulated using the CFD commercial software ANSYS FLUENT[®], which employs the finite volume method. We assumed that the present system comprised a 3D turbulent flow (i.e. channel flow) and a flow with obstacles (i.e. cube flow). Therefore, we considered two different regions: channel flow and cube flow (see figure 3). These numerical tunnels were parametrically tested and considered to be suitable for generating an appropriate turbulence boundary layer to match the conditions of the wind tunnel measurements.

2.2. Turbulence model and governing equations

In this study, a transient DES was employed to render the Reynolds-averaged Navier–Stokes (RANS) equations tractable. In addition, depending on the geometrical complexity and prediction accuracy, the DES has been superior to that of steady or unsteady RANS in terms of the prediction of massive separated flows around complex geometries including the cube arrays (see Squires 2004). For a DES calculation, a large eddy simulation (LES) model calculates the core turbulent region where large unsteady turbulence scales play a dominant role, while a RANS model simulates the near-wall region to reduce the computational cost. Therefore, the DES model denoted as a hybrid RANS/LES model. In this study, the flow calculation in the DES model was also based on the realizable $k - \epsilon$ model in the near-wall region. The transport equations for the turbulence kinetic energy (k) and its dissipation rate (ϵ) are as follows:

$$\frac{\partial}{\partial t}(\rho k) + \frac{\partial}{\partial x_j}(\rho k u_j) = \frac{\partial}{\partial x_j} \left[\left(\mu + \frac{\mu_t}{\sigma_k} \right) \frac{\partial k}{\partial x_j} \right] + G_k + G_b - \rho \epsilon - Y_M \quad (2.1)$$

$$\begin{aligned} \frac{\partial}{\partial t}(\rho \epsilon) + \frac{\partial}{\partial x_j}(\rho \epsilon u_j) &= \frac{\partial}{\partial x_j} \left[\left(\mu + \frac{\mu_t}{\sigma_\epsilon} \right) \frac{\partial \epsilon}{\partial x_j} \right] \\ &+ \rho C_1 S \epsilon - \rho C_2 \frac{\epsilon^2}{k + \sqrt{\nu \epsilon}} + C_{1\epsilon} \frac{\epsilon}{k} C_{3\epsilon} G_b \end{aligned} \quad (2.2)$$

where $C_1 = \max [0.43, \eta/(\eta + 5)]$, $\eta = S(k/\epsilon)$, $S = \sqrt{2S_{ij}S_{ij}}$.

The model constants are given by $C_{1\epsilon} = 1.44$, $C_2 = 1.9$, $\sigma_k = 1.0$, $\sigma_\epsilon = 1.2$ and $C_{3\epsilon} = \tanh |v/u|$, where v and u are the components of the flow velocity parallel and perpendicular to the gravitational vector, respectively.

Among these coupling equations, the eddy viscosity is computed from

$$\mu_t = \rho C_\mu \frac{k^2}{\epsilon} \tag{2.3}$$

where $C_\mu = 1/(A_0 + A_s(ku_*/\epsilon))$, $u_* \equiv \sqrt{S_{ij}S_{ij} + \tilde{\Omega}_{ij}\tilde{\Omega}_{ij}}$ and $\tilde{\Omega}_{ij} = \Omega_{ij} - 2\epsilon_{ijk}\omega_k$, $\Omega_{ij} = \bar{\Omega}_{ij} - \epsilon_{ijk}\omega_k$, where $\bar{\Omega}_{ij}$ is the mean rate-of-rotation tensor viewed in a moving reference frame with an angular velocity ω_k . In addition, the constants are given by $A_0 = 4.04$, $A_2 = \sqrt{6} \cos \phi$, where $\phi = 1/3 \cos^{-1}(\sqrt{6}W)$, $W = S_{ij}S_{jk}S_{ki}/\tilde{S}^3$ and $\tilde{S} = \sqrt{S_{ij}S_{ij}}$, $S_{ij} = (1/2) ((\partial u_j/\partial x_i) + (\partial u_i/\partial x_j))$.

In these equations, G_k represents the generation of turbulence kinetic energy from the mean velocity gradients; G_b is the generation of turbulence kinetic energy from buoyancy, which is not considered in the flow condition, but can be described as follows:

$$G_k = -\overline{\rho u_i u_j} \frac{\partial u_j}{\partial x_i} \tag{2.4}$$

$$G_b = \beta g_i \frac{\mu_t}{Pr_t} \frac{\partial T}{\partial x_i}, \quad \beta = -\frac{1}{\rho} \left(\frac{\partial \rho}{\partial T} \right)_p, \quad Pr_t = 0.85 \tag{2.5}$$

Here Y_M represents the contribution of the fluctuating dilatation in compressible turbulence to the overall dissipation rate. In the DES model, the realizable $k-\epsilon$ RANS dissipation term Y_M is modified by Y_k :

$$Y_k = \frac{\rho k^{3/2}}{l_{des}} \tag{2.6}$$

where $l_{des} = \min(k^{3/2}/\epsilon, C_{des}\Delta)$.

In the equation, C_{des} is a calibration constant of 0.61 used in the DES model and Δ is the maximum local grid spacing. In the flow region, the DES model will approximate the LES model for the case of $C_{des}\Delta < k^{3/2}/\epsilon$; in the reverse case of $C_{des}\Delta > k^{3/2}/\epsilon$, the model will estimate the behaviour of the realizable $k-\epsilon$ model. The realizable $k-\epsilon$ model is an enhancement upon the standard $k-\epsilon$ model because it modifies the dissipation rate (ϵ), improving the models of the separated flow region and complex flow.

2.3. Inlet flow conditions

In order to simulate the turbulent boundary layer at the inlet of the flow domain, the boundary layer was first generated in a channel flow without a cube with a Reynolds number of $Re = 4.6 \times 10^4$ based on the velocity at the cube height. The boundary layer in the domain is continuously regenerated in the channel flow, which is possible because it uses the periodicity boundary condition that combines the inlet with the outlet layer and repeatedly recirculates the flow.

There are essentially two methods for generating the necessary inflow. The first is a statistical method wherein a sequence of random numbers is created and then filtered to yield appropriate statistical properties and spatial correlations (Xie & Castro 2008). The second involves performing a separate ‘precursor’ simulation of a wind environment and sampling the inflow data directly from this (Lim *et al.* 2009).

Parameter (wind tunnel)		Value
Velocity at cube height	U_h	8.1 m s ⁻¹
Boundary layer thickness	δ	0.9 m
Displacement thickness	δ^*	0.158 m
Momentum thickness	θ	0.112 m
Roughness length	z_0	0.24 mm
Reynolds number	Re_h	4.6×10^4
	Re_θ	3.3×10^4
Cube model	$w \times h \times d$	0.15 m \times 0.15 m \times 0.15 m

TABLE 1. Characteristics of undisturbed boundary layer at location of test bodies.

The second method has the desirable property that the generated inflow should naturally contain physically realistic coherent structures without these having to be produced artificially; this is the method adopted in the present work. A similar method was used by Nozawa & Tamura (2002) in their computations of flow over a half-cube. Results from the separated inflow (precursor) simulation were sampled after conditioning for approximately $50h/u_*$ and the samples were averaged spatially over the periodic domain and over the period $20h/u_*$ (see Lozano-Duran & Jimenez (2014) for a discussion of computational domain in the streamwise direction).

Figure 2 presents the (a) streamwise velocity profiles of the mean velocity and (b) turbulence intensity obtained in the channel flow. A fully developed turbulent flow was clearly reproduced in the middle of the domain. A channel flow is usually regarded as the flow in a periodic duct between two walls (i.e. smooth walls in this study), so the current simulation calculated the turbulent flow in the lower half duct by using the symmetry condition. It was specifically designed to regenerate the (rural) atmospheric boundary layer in the channel. The natural wind model used a power law exponent for the mean wind speed profile, α , of approximately 0.14 and a turbulence intensity at the top of the building model, I_u , of approximately 0.18, classified as terrain category-2, open terrain, in AS1170.2-1989 (Australian Standards 1989). The DES model calculations were based on the wind tunnel experiments (hereafter, EXP), which were conducted in the Wind Engineering Research Centre at Tokyo Polytechnic University (TPU) in Japan. Table 1 lists characteristics of the undisturbed turbulent boundary layer at the location of the test bodies.

In order to confirm the feasibility of the boundary layer profiles from the EXP and DES results, they were compared with previous results (i.e. CR, LCH and Jeong & Lim (2008) (hereafter, JL)). As shown in figure 2(a), most of the mean velocity profiles agreed well. However, the mean velocity near the wall (i.e. $z/h = 0-0.4$) of the DES model was somewhat higher than the others, which may be caused by the low-resolution of the mesh grid near the wall in the computational techniques. Regarding the size of the numerical tunnel, two new supplementary calculations were also made (i.e. doubling and tripling the domain height). However, even though the domain sizes are all different (i.e. $4h$, $8h$ and $12h$), the overall mean velocity profiles are almost identical but the velocity profiles of the DES calculation less than a height of $h/2$ becomes a bit faster compared with the others due to the wall modelling and the energy balance of wall shear stresses. Further away from the wall (i.e. $z/h > 0.4$), the mean velocity profiles agree well each other. In addition, the wind profiles in figure 2(a) are highly dependent on the terrain roughness conditions, but in the figure they are similar to the power law profile in which the power exponent α is

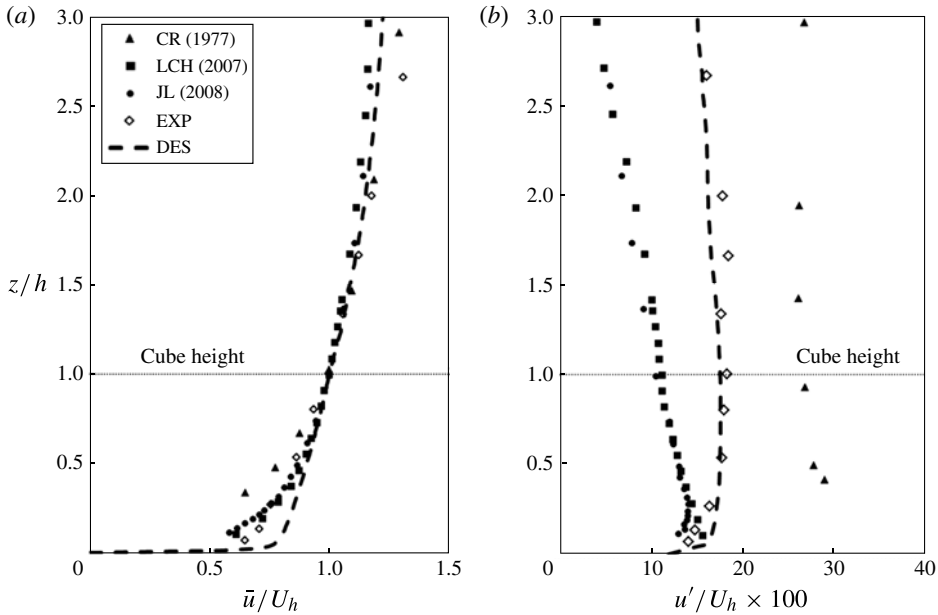


FIGURE 2. Mean velocity (a) and turbulence intensity (b) profiles in the numerical tunnel. The symbols (triangles, squares, circles and diamonds) represent the experimental data. The dashed lines represent the current DES computations.

almost 0.14. An important parameter to characterize the current inlet flow conditions is the mean velocity \bar{u} of approximately 4.2 m s^{-1} at a cube height of 150 mm. Interestingly, although the mean velocity profiles were nearly identical, the turbulence intensity (defined as $I_u = u'/U_h \times 100$, where u' is the fluctuating velocity) profiles that depended on the upstream surface conditions were substantially different. In general, the mean and fluctuating flows are highly dependent on the surface roughness. As shown in figure 2(b), for instance, the comparison between the EXP and the DES shows that they have a similar profile, but are substantially different from other existing results. In particular, LCH and JL evaluated relatively smooth surfaces, while CR made a tunnel experiment on a rough floor. Specifically, the turbulence intensity of the EXP and the DES was approximately 18% at the cube height, which was lower than CR (26.7%) but higher than LCH and JL (11.2% and 12%, respectively). Before proceeding further, it can be easily conjectured that the surface pressure on the bluff body is affected by these different inflow characteristics of the surface roughness. In particular, the turbulence intensity value is a precursor that explains the pressure distributions surrounding them in due course.

3. Results and analysis

3.1. Flow around single cube

In this section, we analyse the flow around the single cube model with a height of 150 mm placed in the open channel to establish the boundary conditions and the size/shape of the model in the full domain, as well as ensuring that the flow characteristics are meaningful and can feasibly resolve the mean and fluctuating components. The blockage ratio (BR) in the current study may be slightly higher

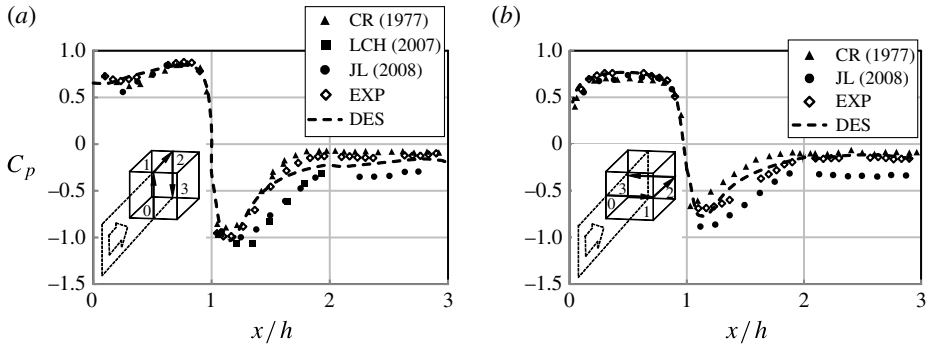


FIGURE 3. Mean surface pressure coefficient around the single cube: (a) along the centreline and (b) at the mid-height.

than expected; BR = 3.57% (single cube), 6.25% (three parallel-aligned cubes), and 3.57% (three tandem cubes) (In the case of speed-up around the obstacle, the effect scales with the ratio of the area of the obstacle's cross-section to that of the frontal cross-section in the domain.). In order to study and understand the full effect of blockage, we performed two new supplementary calculations for the single cube (i.e. doubling and tripling the domain height) in the numerical tunnel. In addition, we have changed the shape of the cube (i.e. rectangular prisms with different ratios); see Gu & Lim (2012). The observed minimum surface pressure coefficient increases with decreasing BR (−0.98 and −0.93), having values closer to the results obtained by CR for a single cube, i.e. −0.92. To the best of the authors' knowledge, it is acceptable, particularly for a wind tunnel experiment. Of course, the tunnel data must be corrected on the basis of blockage correction equations such as those of Maskell (see e.g. Maskell 1963 and Mercker *et al.* 2005).

It is important to simulate the flow around a single cube, which is a fundamental indicator. This was done in a reasonable way, and the results essentially support the rest of the paper. Figure 3 shows the surface pressure variation around the single cube with the previously published data. The coefficient of the mean surface pressure used in the figure is defined as

$$C_p = \frac{p - p_r}{1/2\rho U_h^2} \quad (3.1)$$

where p is the mean pressure around the cube and p_r and U_h are the mean pressure and streamwise velocity at the reference point, respectively. The results both along the centreline (figure 3a) and at the mid-height (figure 3b) are highly dependent on the measurement location x/h (from 0–1, 1–2 and 2–3), which denotes the position around the model normalized by the cube height as shown on the left in each figure. The results indicate that the mean pressure coefficient profiles from DES and EXP are in better agreement with the CR results than those from LCH and JL. However, there is some scatter in the measured data, which was explained above (i.e. it is due to the different turbulence levels). Their study reported that the higher upstream turbulence levels led to a much earlier reattachment as well as an earlier pressure recovery in the far downstream from the top and side surfaces of the bodies. As shown in figure 3, the values of the data from the EXP and DES are in between the values of CR and JL from the top and side surfaces, which is undoubtedly due to the different turbulence intensity values (i.e. see figure 2b). In addition, as pointed out earlier, the maximum

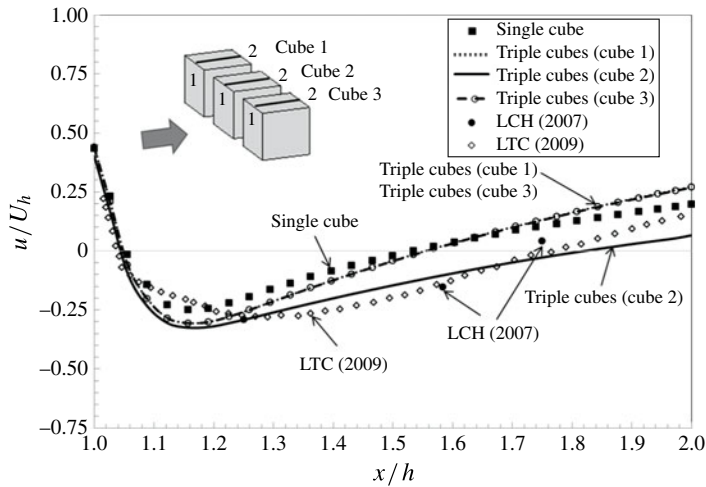


FIGURE 4. Mean axial velocity profiles directly above the top surface ($z/h = 1.01$) of three parallel-aligned cubes ($G = 0.5h$) with a 0° azimuth angle.

negative pressures occur just beyond the separation point (directly to the right-hand side of the position $x/h = 1$) of the top and side surfaces and are followed by a substantial pressure recovery associated with the reattachment process. In figure 3(a), the mean surface pressure along the centreline of the single cube has a typical shape and agrees remarkably well with the EXP and CR results, whereas, because of the lack of the data points in the EXP, the surface pressure at the centre of the mid-height seems to be scattered; however, it looks reasonable. Regarding the feasibility and reliability of the current work, we believe this section explains the uncertainty of the data subsequently presented in this paper, which describe the flow around the consecutive cubes placed in the same turbulent boundary layer.

3.2. Flow around three parallel-aligned cubes: effect of azimuth angle

If a group of bodies are placed in close proximity or are aligned in series or parallel, the flow around and between the bodies undergoes interference, inducing a complicated turbulent flow. Owing to these interference effects, the flow around three parallel-aligned cubes is more complicated than around a single cube. Figure 4 shows the mean axial velocity profiles along the centreline immediately above the top surface ($z/h = 1.01$) of the single cube and the three parallel-aligned cubes. For the case of the flow around the three parallel-aligned cubes, the gap distance G between the cubes is first set to $0.5h$ and the wind is set to a normal incidence on the cubes (i.e. the azimuth angle is 0°). The velocity profiles of cubes 1, 2 and 3 are all dependent on the measurement location x'/h (from 1–2), where $x'/h = 1$ denotes the leading edge of the top surface of the cube shown in the figure. In addition, the results obtained from the DES are also compared with the existing results of LCH and LTC, which showed a typical mean velocity distribution around the single cube in both the wind tunnel and the LES simulations. As shown in figure 4, the normalized velocity u/U_h versus x/h tends to rapidly drop to approximately 1.1 owing to the separation of the leading edge and then gradually increases downstream of the cube top surface. While the velocity increases far downstream, it experiences a velocity

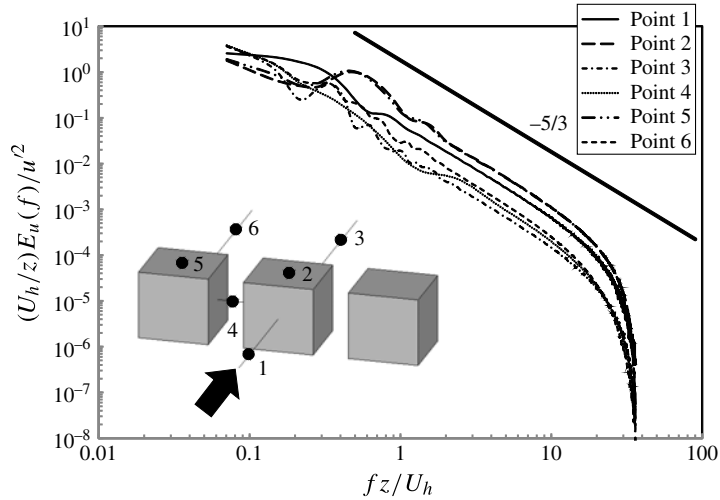


FIGURE 5. Velocity spectra at various measurement locations of three parallel-aligned cubes ($G = 0.5h$) with a 0° azimuth angle.

change from negative to positive so that the fluid particle from the separation region reattaches to this point (i.e. reattachment point).

Regarding the single cube, the reattachment length ($x'/h = 1.54$) is shorter than that of LCH and LTC ($x'/h = 1.75$). As previously pointed out, these differences are likely caused by the different level of turbulence intensities at the inlet. The higher upstream turbulence disturbs the streamlines separated from the leading edge in the recirculation region, so this fluctuation tends to promote the earlier attachment of the separated streamlines and shortens the reattachment length even though there is always separation flow from the leading edge of the cube. In this study, the turbulence intensity is 18%, whereas it is approximately 12% in LCH and LTC, as shown in figure 2(b). Regarding the velocity profiles of cubes 1, 2 and 3, the figure clearly indicates that the reattachment length from the leading edge on the centre cube, cube 2, occurs near $x'/h = 1.8$, whereas it occurs near $x'/h = 1.56$ for cubes 1 and 3 (i.e. the neighbouring cubes). Interestingly, owing to the gap spacing, the reattachment length of the neighbouring cubes occurs at a length 18% shorter than for the centre cube. As a first finding in this paper, this is emphasized by the fact that the recirculation region on the top surface of the centre cube reaches further downstream because of the interference effects of the neighbouring body, which appears to be a 2D wide structural body (i.e. see JL).

In order to observe the spectral characteristics around the three parallel-aligned cubes (with $G = 0.5h$ and an azimuth angle of 0°), the power spectra were analysed at various measurement locations (from point 1 to 6). As shown in figure 5, the power spectra observed in the fully developed turbulent boundary layer exhibit a typical shape, which helps to understand the large- and small-structure turbulence flows and the energy transfer process from large to small scales (i.e. the cascade process). In the small-scale region (i.e. the high-frequency range), the spectra linearly decrease with increasing non-dimensional frequency, ending with a sudden drop that is due to the inherent limitation of the grid size and the domain. Overall, the profiles of the energy spectra are reasonably comparable. In particular, the solid line of point 1 represents the velocity spectra of an upstream point in the oncoming

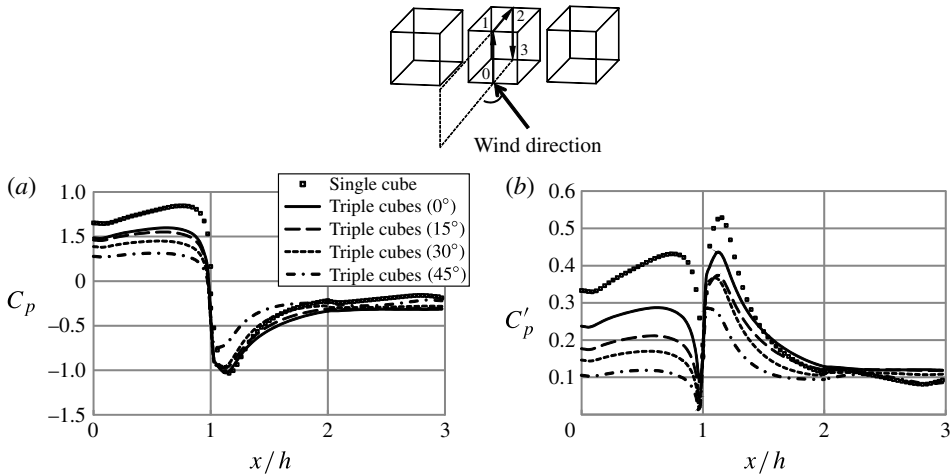


FIGURE 6. Pressure variation along the centreline around three parallel-aligned cubes ($G=0.5h$) under different azimuth angles: (a) mean pressure coefficient and (b) fluctuating pressure coefficient.

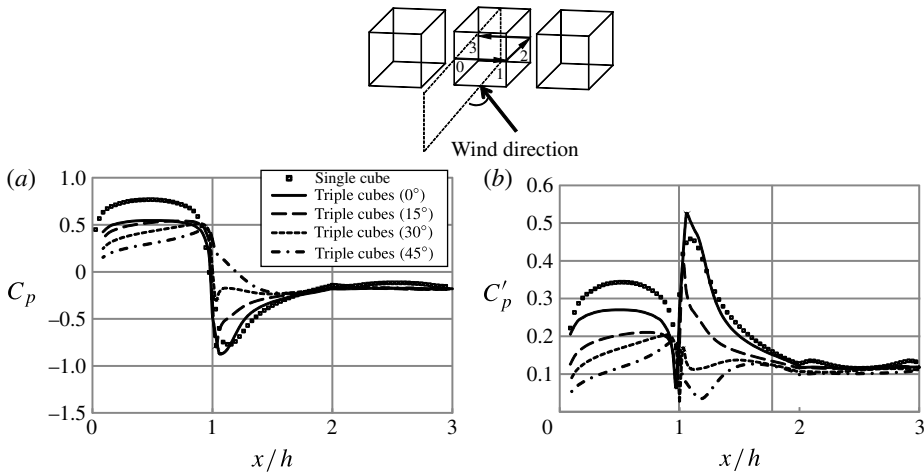


FIGURE 7. Pressure variation around three parallel-aligned cubes ($G = 0.5h$) at the mid-height for different azimuth angles: (a) mean pressure coefficient and (b) fluctuating pressure coefficient.

boundary layer; it contains the history of the simulated oncoming flow. The other dotted lines represent the points on the side and the back of the cubes. In the figure, the overall power spectra at different locations all have a slope of $-5/3$ in the inertial subrange region spanning $fz/U_h = 1-10$. In addition, all of the velocity spectra drop rapidly when fz/U_h is over approximately 25. These results are also observed and discussed in LCH.

Figures 6 and 7 show the pressure variation obtained from the DES of the three parallel-aligned cubes with respect to the azimuth angle (i.e. 0, 15, 30 and 45°). The results of the flow around three parallel-aligned cubes are also compared with the single cube with a 0° azimuth angle. Although the azimuth angle was varied, the

gap distance G was maintained at $0.5h$. In addition, this study aims to understand the surface pressure variation of the centre cube, so it is plotted with respect to the same coordinate, x/h . With the variation of the azimuth angle, as clearly expected, the surface pressure changes substantially owing to the sheltering effect, particularly in the range of the frontal area and the separated leading edge on the top surface. Figure 6 shows the mean (C_p) (figure 6a) and the fluctuating (C'_p) (figure 6b) pressure coefficients along the centreline of the centre cube. As shown in figure 6(a), regardless of the azimuth angle, the overall distributions of the surface pressure coefficients have similar profiles as the previously published data: positive values at $x/h=0-1$, negative values at $x/h=1-3$ and approximately constant values on the leeward side, $x/h=2-3$. As mentioned earlier, the surface pressure tends to vary as the azimuth angle changes; it is especially sensitive on the front and top faces. On these faces, the surface pressure decreases as the azimuth angle increases. Meanwhile, the surface suction pressure on the top and rear faces gradually decreases with an increasing azimuth angle. As the azimuth angle increases, the suction peak has a minimum value near the leading edge of the cube, and then the peak moves closer to the leading edge. The fluctuating pressure distribution is an important factor for the safety and design optimization of the structure. In figure 6(b), the fluctuating pressure in the separation region (immediately right of the position $x/h=1$) on the top surface exhibits a rapid increase, a maximum peak and, finally, an exponential decay. Furthermore, with the increasing azimuth angle, the fluctuating pressure coefficient decreases not only on the front face but also on the top and rear faces. This indicates that as the wind direction changes, the 2D separation at the leading edge becomes 3D complicated flow. It should also be noted that, depending on the oncoming wind angle, the mean and fluctuating pressures have a substantial impact on the stability of the buildings or structures.

Figure 7 describes the same arrangement as figure 6, but it shows the surface pressure variation at the mid-height of the centre cube. Both the mean (figure 7a) and the fluctuating (figure 7b) pressure coefficients tend to exhibit a similar shape with a changing azimuth angle. However, as compared with figure 6, the distributions in figure 7 have a larger variation, especially for the side face. In figure 7(a), for example, as the azimuth angle increases, the mean surface pressure at the side face rapidly changes at the leading edge. As oncoming wind begins to face the side of the centre cube the sharp leading edge does not generate a separated flow but faces normal to the flow and has a positive pressure. However, in figure 7(a), the mean pressure coefficient for a portion of the side face ($x/h=1-1.2$) changes drastically from negative to positive owing to the neighbouring cubes. In addition, as the side face turns to face a direction normal to the wind, the surface pressure on the side gradually increases. In fact, the neighbouring cubes interfere and deter the wind from blowing on the front face and yielding the valley flow. Thus, the overall pressure distribution is not exactly symmetrical in the range of $x/h=0-2$. Furthermore, with an increase in the azimuth angle, the fluctuating pressure on the front and top faces weakens; the peak fluctuating pressure occurs on the corner of the leading edge at approximately $x/h=1$.

3.3. Flow around three parallel-aligned cubes: effect of gap distance

Figure 8 shows the axial mean velocity profiles directly above the top surface ($z/h=1.01$) of the centre cube, which is in close proximity to two neighbouring cubes with increasing gap distances ($G=0.5h, 1.0h$ and $1.5h$). The velocity profiles are calculated

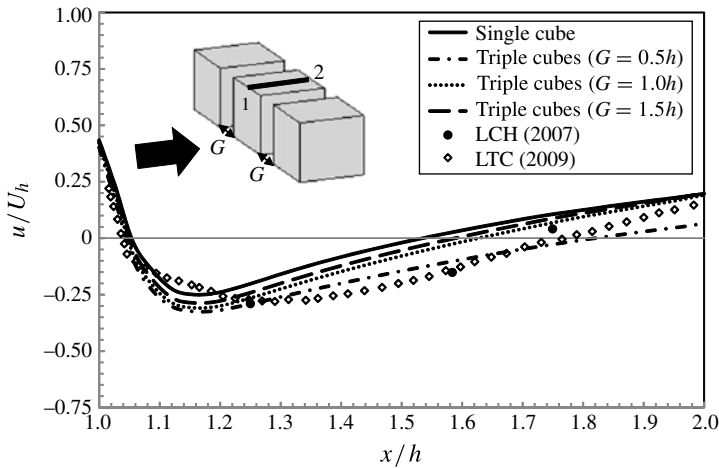


FIGURE 8. Mean axial velocity profiles directly above the top surface ($z/h = 1.01$) on the centre cube of three parallel-aligned cubes for different gap distances.

with the DES for the case of an azimuth angle of 0° and they are dependent on the measurement location x'/h (from 1–2) of the centre cube, as shown in the figure. In addition, the velocity profiles of the three parallel-aligned cubes with different gap distances are also compared with that of the single cube, as well as the existing results of LCH and LTC. From their results, the single cube exhibits the shortest reattachment length, whereas the three parallel-aligned cubes with a gap distance of $G = 0.5h$ has the longest reattachment length. This clearly indicates that the reattachment length on the top of the single cube, represented in this figure as $G = \infty$, decreases as the gap distance increases in the gap distance range of $0.5h < G < 1.5h$. Even though the gap was not a long distance away, the value $G = 3$ was fairly effective when considering the condition of a single cube. This method was not appropriate for obtaining the overall tendency over the cubes, but a different view of this effect can be observed in a future study.

As shown in figure 9, in order to understand the overall characteristics of the flow around a group of cubes, the isosurface contours of the vorticity are calculated with different gap distances: (a) $G = 0.5h$; (b) $G = 1.0h$; and (c) $G = 1.5h$. The dark-shaded block indicates the cube model and the grey isocontour is the Q-criterion (II) (see also LTC), which is defined as

$$II = -L_{ij}L_{ji} \quad (3.2)$$

where $L_{ij} \equiv \partial u_i / \partial x_j$ and is a measure of the regions of flow dominated by rotation rather than shear or stretching. In this study, the Q-criterion is the same value ($II = 600$) in the entire domain (i.e. isosurface contour) for different gap distances. These visualizations qualitatively indicate the features of the flow, which can also be seen in some existing literature, for example, in Shah & Ferziger (1997) and Yakhot *et al.* (2006). As shown in figure 9, although it is not very noticeable, the vortex structures are fairly different with a change in the gap distance. In particular, as the gap increases, the necklace vortices in front of the cube arrays separate into individuals and merge between cubes. They finally disappear because of the speed increase in the gap space. The vortex structure is not revealed in these visualizations, but a draft picture is seen of the flow around cube arrays, which was not observed in previous papers.



FIGURE 9. Isosurface contours of the vorticity around three parallel-aligned cubes for different gap distances: (a) $G = 0.5h$; (b) $G = 1.0h$; and (c) $G = 1.5h$.

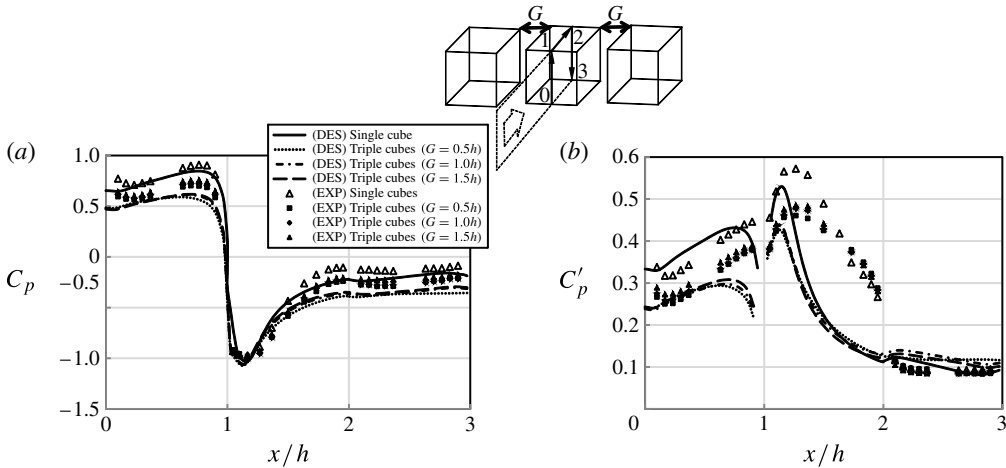


FIGURE 10. Pressure variation along the centreline around three parallel-aligned cubes for different gap distances: (a) mean pressure coefficient and (b) fluctuating pressure coefficient.

Figure 10 shows the pressure variation around the three parallel-aligned cubes with respect to the gap distance ($G = 0.5h, 1.0h, 1.5h$, and ∞), which consists of the mean (C_p) (figure 10a) and fluctuating (C'_p) (figure 10b) pressure coefficients along the centreline of the centre cube. The marker symbols represent the EXP data and the solid or dotted lines represent the DES data; the draft figures denoting the measurement points around the models are shown above the graph. Although the EXP and DES results differ slightly, the comparison of both profiles indicates nearly equivalent pressure variations. In figure 10(a), because the neighbouring cubes are in close proximity to the centre cube with different gap distances, the overall mean pressure distributions have a similar shape of the single cube. In addition, the group of cubes has a consistently lower surface pressure than that of the single cube. For instance, at the separation points (i.e. around $x/h = 1$), the mean pressure coefficients are generally similar, but the flow around the single cube recovers faster than that of the three cubes. This is caused by the effect of the gap flow between the centre cube and the neighbouring cubes. The flow around the centre cube accelerates between these gaps, delaying the pressure recovery. Furthermore, as shown in figure 10(b), the surface fluctuating pressure has a substantial peak at the leading edge region of the top surface, with a maximum r.m.s. of approximately 0.55. In the figure, it could

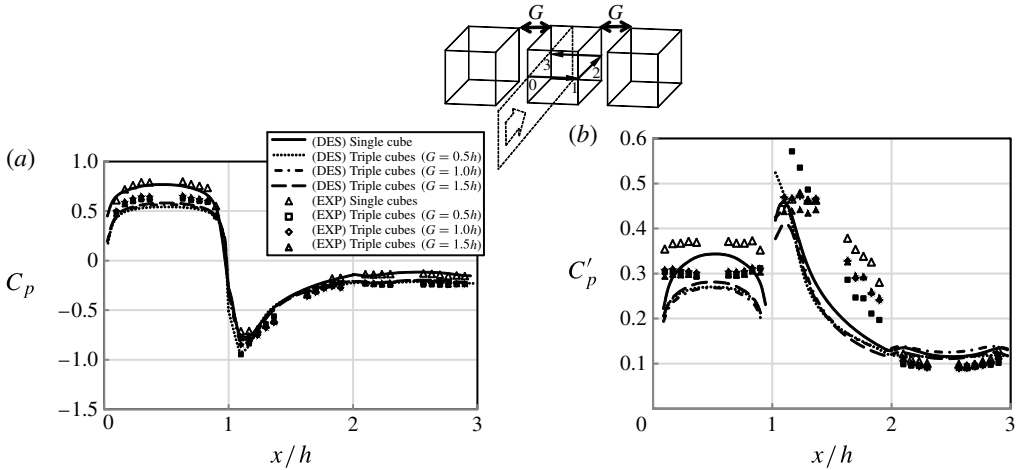


FIGURE 11. Pressure variation at the mid-height around three parallel-aligned cubes for different gap distances: (a) mean pressure coefficient and (b) fluctuating pressure coefficient.

be argued that the fluctuating pressure in the EXP and DES results has a substantial discrepancy, particularly on the top of the cube. We could conjecture that this seems to be an issue with the DES model, which yields a strong suction pressure on the top surface. This is also observed in LTC. Interestingly, we also found that the fluctuating pressure of the single cube is generally higher than that of the three cubes, which could be caused by an interference effect of the neighbouring cubes making a portion of the side flow move over the cubes, where a strong suction pressure is generated.

Figure 11 shows the pressure variations at the mid-height of the centre cube obtained from the EXP and the DES. As shown in figure 11(a), the mean pressure variation trend is similar to that in figure 10(a). However, in the region of $x/h = 1.1$ – 1.2 , there are some minor differences in terms of the mean surface pressure with respect to the gap distance. As the distance between the cubes increases, the lowest peak of the mean pressure coefficient gradually recovers. For example, the lowest peak of the mean surface pressure reaches approximately -0.95 at $G = 0.5h$ and -0.75 for the single cube. In addition, the interference effects dominate the fluctuating surface pressure at the mid-height of the centre cube. Interestingly, as shown in figure 11(b), the variation in the surface pressure tends to be substantial close to the leading edge, $x/h = 1$, which is not observed in the pressure profiles along the centreline of the centre cube. That is, the maximum peak of the fluctuating pressure at the leading edge does not appear for the single cube or three parallel-aligned cubes with $G = 1.0h$ and $1.5h$, but there is a predominant peak for the three parallel-aligned cubes with $G = 0.5h$. The magnitude and location of the DES results were not exactly consistent with those for the EXP results, but the peak was also observed in the EXP results. This is a significantly important fact because it shows that there is a critical point for increasing the fluctuating pressure, which will be further used for the design of the deployment and arrangement of neighbouring buildings and structures. This finding also highlights the fact that, depending on the gap distance, the building arrays have interference effects on each other. Thus, there should be an optimal design.

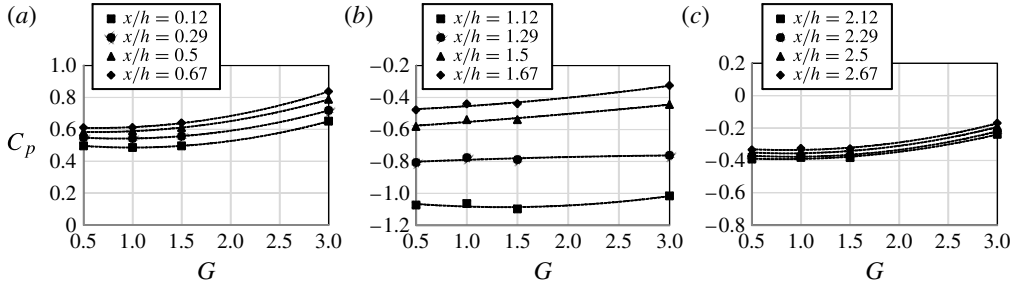


FIGURE 12. Mean pressure at several points along the centreline for different gap distances: (a) the front face; (b) the top face; and (c) the rear face.

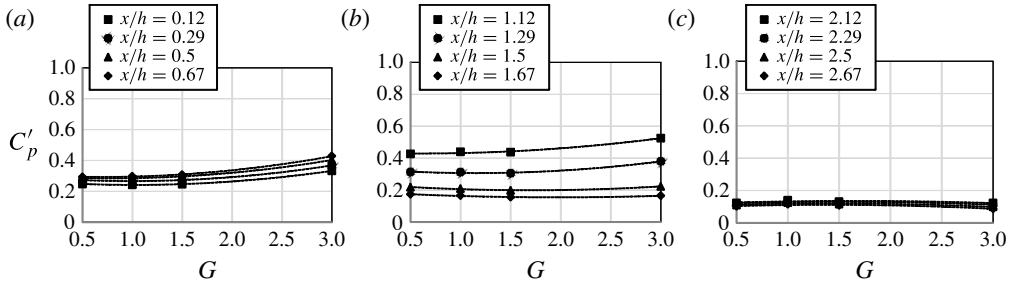


FIGURE 13. Fluctuating pressure at several points along the centreline for different gap distances: (a) the front face; (b) the top face; and (c) the rear face.

In order to observe the effect of the gap distance, figures 12 and 13 show the mean and fluctuating pressure coefficients, respectively, around the three parallel-aligned cubes at several points on the front (figures 12a and 13a), top (figures 12b and 13b), and rear (figures 12(c) and 13(c)) faces of the centre cube with respect to various gaps: $0.5h$, $1.0h$, $1.5h$ and ∞ . Although this assumption can be used as a rule of thumb, it would be beneficial to use the surface pressure of the gap for $G = 3$ as the gap distance for $G = \infty$. As shown in figures 12(a) and 13(a), the mean and fluctuating pressures, respectively, at several points along the centreline of the front face increase with increasing gap distance. These results imply that a narrow gap between the cubes induces valley flow, resulting in a higher-speed and lower-pressure region, whereas a wide gap tends to mimic single cube flow, decreasing the wind speed and increasing the surface pressure. However, this variation is not suitable to explain the pressure variations for the top and rear faces. As shown in figures 12(b) and 13(b), the pressure variations along the centreline of the top face in the upper and lower range of $x/h = 1.5$ are substantially different. For instance, in the first half of the top surface (i.e. the range $x/h < 1.5$), the mean pressure coefficient remains approximately constant as the gap increases. In the second half of the top surface (i.e. the range $x/h \geq 1.5$), the mean pressure coefficient noticeably increases with an increasing gap. These data enable a comprehensive understanding of the effect of the flow separation and reattachment on the pressure variations of cube surfaces (see figure 4). That is, the separation region on the first half of the top surface seems to prevent the mean pressure from remaining a constant value, compared with that on the second half. In addition, figures 12(c) and 13(c) show the mean and

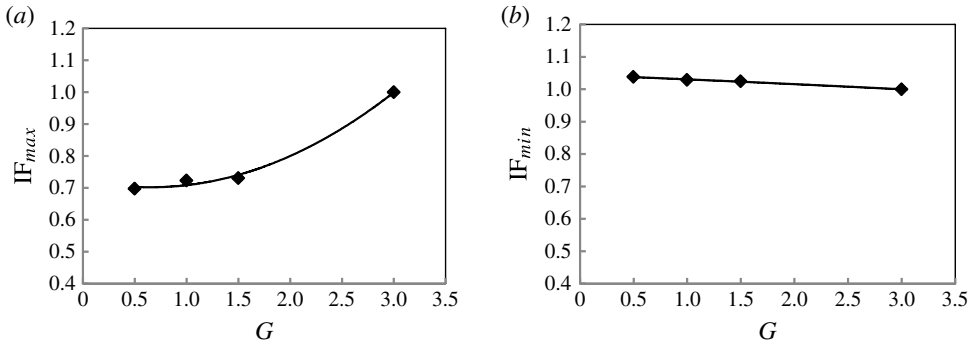


FIGURE 14. Non-dimensional IF variations along the centreline with respect to gap distance: (a) for the maximum mean pressure coefficient and (b) for the minimum mean pressure coefficient.

fluctuating pressures, respectively, along the centreline of the rear face. The mean pressure variation exhibits a similar trend as the front face; the pressure coefficients increase as the gap distance increases. However, the fluctuating pressure on the rear face remains constant.

In order to explain these interference effects, more adequate parameters must be defined. The non-dimensional IF is a good candidate, which was originally introduced by Saunders & Melbourne (1979). The IF is calculated to evaluate the interference effects of the neighbouring cubes, which is defined as

$$IF = \frac{\text{Surface pressure of the cube with neighbouring cubes}}{\text{Surface pressure of the cube without neighbouring cubes}} \tag{3.3}$$

In this study, to investigate the gap distance effects on the maximum and minimum surface pressures, the IFs (i.e. symbolized as IF_{max} and IF_{min}, respectively) are defined as

$$IF_{max} = \frac{C_{p,max}(\text{centre cube of three parallel – aligned cubes})}{C_{p,max}(\text{single cube})} \tag{3.4}$$

$$IF_{min} = \frac{C_{p,min}(\text{centre cube of three parallel – aligned cubes})}{C_{p,min}(\text{single cube})} \tag{3.5}$$

Figure 14 shows the IF_{max} and IF_{min} along the centreline of the centre cube for different gap distances. As mentioned previously, G = 3 is approximated as the gap distance G = ∞; in this case, the IF is unity. As shown in figure 14, the IF_{max} increases and the IF_{min} decreases as the gap distance increases. That is, as the gap distance approaches G = 3 (i.e. a single cube, ∞ as considered), both IF_{max} and IF_{min} should have values close to one, because the surface pressures should be the same for the cube with a neighbouring cube a long distance away and that without neighbouring cubes. Interestingly, when the gap between the buildings is wide, the positive peak value of the mean pressure on the centre cube grows exponentially, whereas the minimum value is inversely proportional to the gap distance. In this regard, the maximum and minimum surface pressures tend to have unique variations with respect to the gap distance when one is considering the construction design of consecutive buildings.

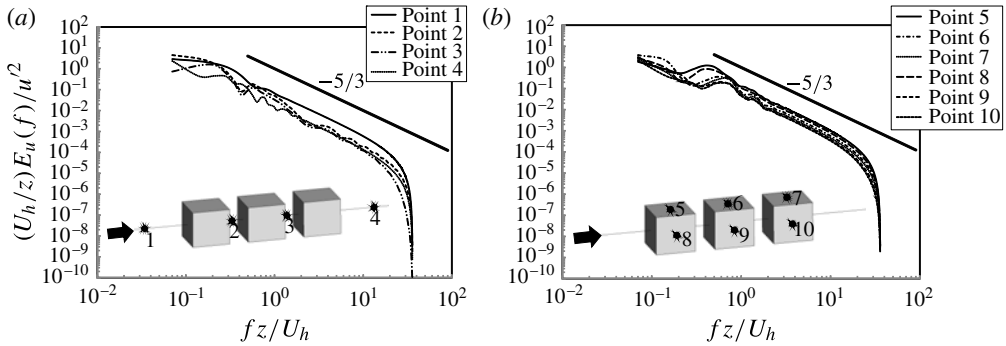


FIGURE 15. Velocity spectra comparison for different measurement locations of three tandem cubes ($G=0.5h$) for a 0° azimuth angle.

3.4. Flow around three tandem cubes

For the flow around three parallel-aligned cubes, the neighbouring cubes have a diverse effect on the interference depending on the gap distance. However, if the group of cubes has a tandem arrangement, it is not easy to judge how the interference affects the pressure variation around cubes, because the pressure variation around the second and third cubes is estimated to be negligible due to the separation of the leading edge of cube 1. This is an important design parameter for ensuring an optimal arrangement of a group of bluff bodies. Figure 15 presents the velocity spectra for three tandem cubes. Figure 15(a) shows the velocity spectra of several salient points in front of the cubes (point 1), between the cubes (points 2 and 3) and behind the cubes (point 4). In addition, figure 15(b) shows some unique points on the top (points 5, 6 and 7) and side (points 8, 9 and 10) faces of the three tandem cubes. The velocity spectra exhibit gradual changes that depend on the location. In particular, in the low-frequency region, the spectral peaks, which are not clearly shown, are located at approximately $fz/U_h < 1$. The oncoming flow (i.e. see point 1) does not seem to have any peaks with particular frequencies, which is similar to points 2–4. However, as shown in figure 15(b), spectral peaks close to the side and top surfaces are observed at a higher frequency of approximately $fz/U_h = 1$, which seem to be caused by the breaking of the oncoming wind flow into small-scale turbulence yielding a higher frequency of eddies. Furthermore, the spectral decay has an inertial $-5/3$ region from $fz/U_h = 1$ to 10 and a rapid drop when $fz/U_h > 25$, which was explained previously.

Figure 16 shows the axial mean velocity profiles immediately above the top surface ($z/h = 1.01$) of the three tandem cubes for different gap distances ($G=0.5h, 1.0h, 1.5h$ and ∞). In the figure, the coordinate of x'/h is plotted in the range between the leading and trailing edges (from 1–2) on the top surface of the single cube and the three consecutive cubes, cubes 1, 2 and 3, denoted in the top figure. The results obtained from DES are also compared with the results of LCH and LTC. The flows around both the single cube and cube 1 for all three gap distances have similar reattachment points near $x'/h = 1.56$ (see the velocity in figure 15; note that the three lines on the graph approximately overlap). These results indicate that the gap distance has negligible influence on the reattachment of the three tandem cubes after cube 1. As shown in the figure, the flow around cubes 2 and 3 exhibits no separation or reattachment. Therefore, the velocity profiles are substantially different from that of cube 1. However, it also clearly seen that there are gap-dependent velocity variations

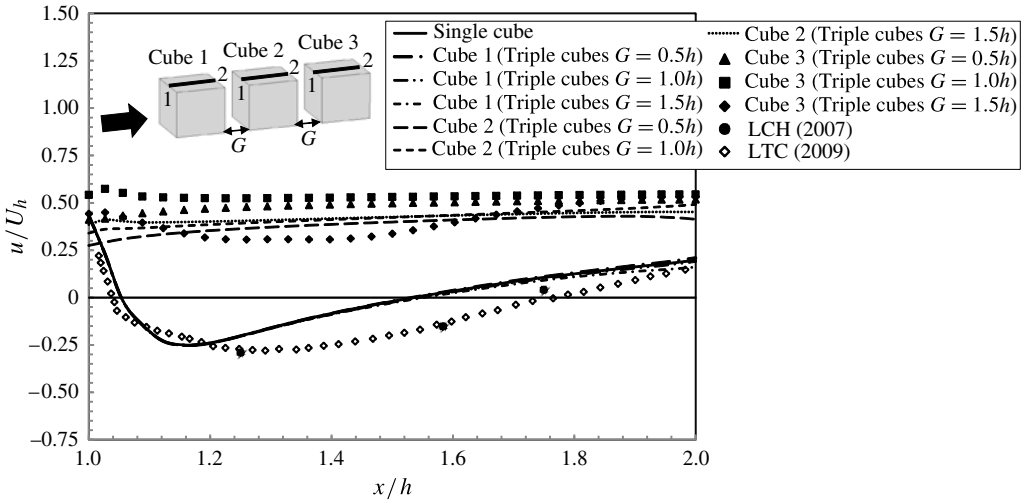


FIGURE 16. Mean axial velocity profiles immediately above the top surface ($z/h = 1.01$) of three tandem cubes for different gap distances.

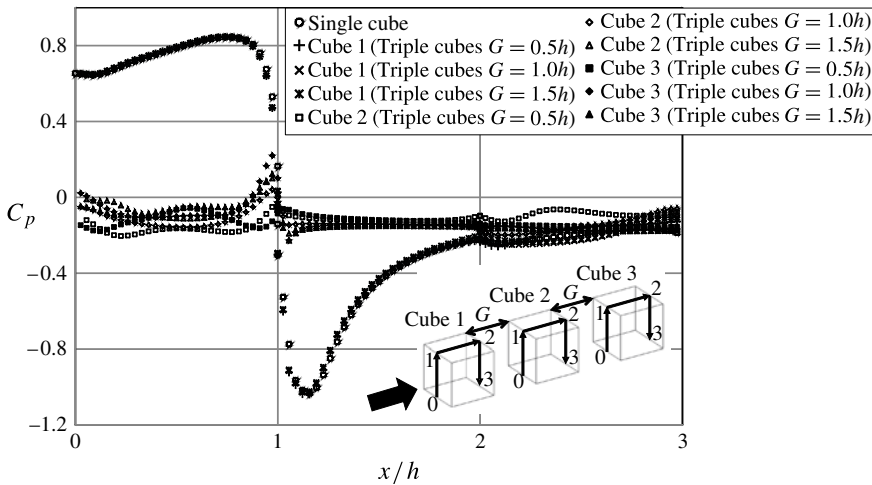


FIGURE 17. Mean pressure variation along the centreline around three tandem cubes for different gap distances.

around cubes 2 and 3. Therefore, although the gap distance has a negligible influence on the reattachment around the first cube, it has a substantial effect on the flow variations around the second and third tandem cubes.

Figures 17 and 18 show the centreline and mid-height surface pressure variations, respectively, around the three tandem cubes for different gap distances. In the figures, most of surface pressure profiles are fairly consistent and constant (i.e. slightly less than zero) because the upstream cube 1 blocks most of the oncoming flow and generates a sheltering effect. Thus, the separate flow from cube 1 forms an external shield that prevents pressure restoration over the two downstream cubes. In this regard, cubes 2 and 3 do not have typical pressure distributions, whereas cube 1

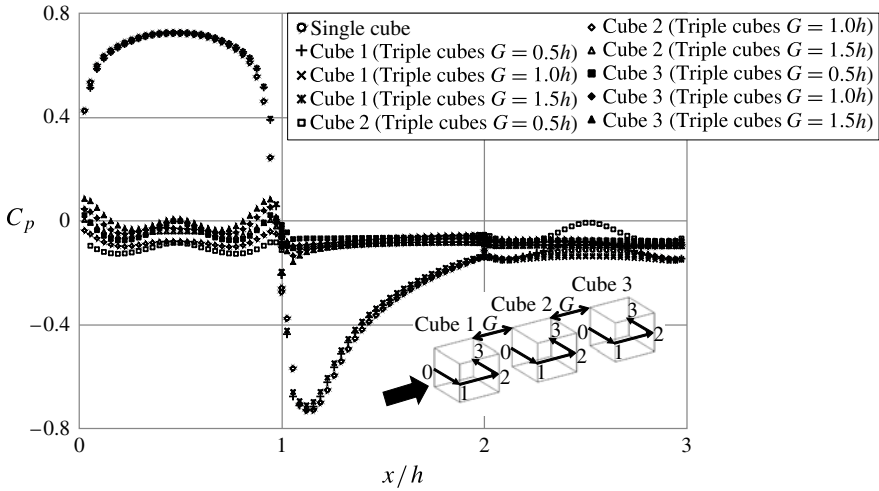


FIGURE 18. Mean pressure variation at the mid-height around three tandem cubes for different gap distances.

tends to have a pressure distribution that is typical for the flow around a single cube. Overall, the mean pressures on cubes 2 and 3 are generally smaller than that of a single cube. However, the comparison of the pressure profiles of the single cube, cube 1 (see $G = 0.5h, 1.0h$ and $1.5h$) in both figures 17 and 18, indicates that there is almost no difference between the pressure profiles of the single cube and cube 1. Although there are two consecutive cubes directly in the wake of cube 1, the flow separation and reattachment of cube 1 and the single cube must be nearly equivalent. This indicates that the cubes behind cube 1 do not affect its pressure variation; if there are any interference effects, they are minor. For cubes 2 and 3, the gap distance substantially influences the pressure variation. As the gap distance increases, the mean pressure coefficients along both the centreline and the mid-height of the cubes increase. Therefore, an important conclusion is that the gap distance has little effect on the pressure variation of the first cube (i.e. cube 1), but it has a significant effect on the pressure variations of the consecutive cubes in a tandem arrangement.

4. Conclusions

Owing to the interference effects of the neighbouring cubes, a detailed analysis of the flow structure around three consecutive wall-mounted cubes is considerably complicated. This paper presents transient DES calculations around a single cube, three parallel-aligned cubes and three tandem cubes placed in a deep turbulent boundary layer. In addition, the DES results are also compared with the EXP results. We mainly focused on the effects of different azimuth angles and different gap distances, and there are numerous key points here. We summarize our major findings as follows. (i) For flows and wind loads around multiple obstacles, the gap distance and azimuth angle are significantly important and can be used for the design of the deployment and arrangement of neighbouring buildings and structures. (ii) Despite the lack of wind tunnel data, there are new mean flow data, as well as fluctuating quantities, for the single- and triple-cube cases. In addition, (iii) this paper includes much more reasonable and improved mean and turbulence quantities, as well as the

interference effect of multiple obstacles according to the DES calculation. (iv) We observed that the peak fluctuating pressure and gap distance have a substantial effect on the central cube of the three parallel-aligned cubes but not on a single cube; this phenomenon had never been achieved before. This study can be summarized as follows.

(a) The DES results regarding the surface mean pressure are in overall agreement with the EXP results, including the existing results of other papers (e.g. CR, LCH and JL). This confirmed the accuracy and reliability of this study.

(b) Regarding the flow around the three parallel-aligned cubes with a gap distance of $0.5h$, the mean reattachment length of the neighbouring cubes occurs at a relatively at shorter length than of the centre cube.

Furthermore, the mean reattachment length after the centre cube decreases as the gap distance increases. However, when the three cubes are placed in a tandem arrangement, the mean reattachment length of the first cube does not change much as the gap distance increases. In addition, the flows around the second and third cubes do not separate or reattach, but the gap distance has a substantial effect on the velocity variations.

(c) Depending on the variation of the azimuth angle, the surface pressure profiles on the centre cube of the three parallel-aligned cubes show that both the surface suction pressure at $x/h = 1-3$ and the positive pressure at $x/h = 0-1$ weaken with an increasing azimuth angle. In particular, on some of the side faces ($x/h = 1-1.2$), the mean pressure coefficient can even change from a negative value to a positive value. In addition, the largest fluctuating pressure occurs at the position near $x/h = 1$. Furthermore, all surface fluctuating pressures decrease as the azimuth angle increases.

(d) The mean pressure coefficient of the centre cube placed in the three parallel-aligned cubes is generally lower than that of the single cube and tends to increase in polynomial shape depending on the gap distance for the case of an azimuth angle of 0° . The peak fluctuating pressure along the centreline of the single cube is higher than that of the three parallel-aligned cubes. For the case of the mid-height of the centre cube, while a peak fluctuating pressure does not appear in the flow around the single cube, it appears at the centre cube of the three parallel-aligned cubes with a gap distance of $0.5h$. In particular, these facts highlight the importance of interference effects for designing neighbouring structures of buildings. In addition, once the gap distance changes, the vortex of the structures are also substantially altered. For example, with increasing gap distance, the vortex in front of the three parallel-aligned cubes separates into individual shields.

(e) Regarding the fluctuating pressure, the maximum peak at the leading edge does not appear for the single cube and three parallel-aligned cubes with $G = 1.0h$ and $1.5h$, but there is a predominant peak for the three parallel-aligned cubes with $G = 0.5h$. The magnitude and location of the peak are significantly important because they show that there should be a critical point to increase the fluctuating pressure, which highlights the fact that, depending on the gap distance, buildings in an array have interference effects on each other. Thus, there should be an optimum design.

(f) The gap distance plays an important role in the pressure variation of the three parallel-aligned cubes, but it has a negligible effect on the first cube for a flow passing three tandem cubes. However, it has a significant influence on the consecutive cubes (i.e. the cubes are directly influenced by the wake of the first cube). For example, with increasing gap distance, the mean pressure coefficients both along the centreline and at the mid-height of the second and third cube tend to increase.

More comparisons are still required to validate the conclusions. However, this study already includes some crucial points for understanding the interference effects

to designing single and multiple structures. In addition, as this study focuses on the gap distance effects, more investigations for at least $G > 1.5h$ are required as further research. In the near future, we will work to conduct a complementary test to obtain a higher reliability regarding the interference effects among multiple bodies.

Acknowledgements

The authors wish to thank Ms. Dan Gu and Mr. Young Tae Lee (School of Mechanical Engineering, Pusan National University) for their crucial help. This work was supported by the Human Resources Development of the Korea Institute of Energy Technology Evaluation and Planning (KETEP) grant funded by the Korea government Ministry of Knowledge Economy (grant nos 20124010203230 and 20114010203080). In addition, this research was supported by Basic Science Research Program through the National Research Foundation of Korea (NRF) funded by the Ministry of Education, Science and Technology (grant nos 2013005347).

REFERENCES

- ARIE, M., KIYA, M., MORIYA, M. & MORI, H. 1983 Pressure fluctuations on the surface of two cylinders in tandem arrangement. *Trans. ASME J. Fluids Engng* **105**, 161–167.
- Australian Standards 1989 SAA loading code Part 2: Wind loads. AS1170.2-1989.
- BAILEY, P. A. & KWOK, K. C. S. 1985 Interference excitation of twin tall buildings. *J. Wind Engng Ind. Aerodyn.* **21**, 323–338.
- BEARMAN, P. W. & WADCOCK, A. J. 1973 The interaction between a pair of circular cylinders normal to a stream. *J. Fluid Mech.* **61**, 499–511.
- CASTRO, I. P. & ROBINS, A. G. 1977 The flow around a surface mounted cube in uniform and turbulent streams. *J. Fluid Mech.* **79**, 307–335.
- GU, D. & LIM, H. C. 2012 Effects of aspect ratio and wind direction on flow characteristics around rectangular obstacles. In *10th UK Conference on Wind Engineering, Southampton, 10–12 September*, pp. 163–166.
- HUI, Y., TAMURA, Y. & YOSHIDA, A. 2012 Mutual interference effects between two high-rise buildings models with different shapes on local peak pressure coefficients. *J. Wind Engng Ind. Aerodyn.* **104–106**, 98–108.
- HUI, Y., YOSHIDA, A. & TAMURA, Y. 2013 Interference effects between two rectangular-section high-rise buildings on local peak pressure coefficients. *J. Wind Engng Ind. Aerodyn.* **37**, 120–133.
- JEONG, T. Y. & LIM, H. C. 2008 Study on the generation of turbulent boundary layer in wind tunnel and the effect of aspect ratio of a rectangular obstacle. *Trans. Korean Soc. Mech. Engng* **32**, 791–799.
- KHANDURI, A. C., STATHOPOULOS, T. & BEDARD, C. 1998 Wind-induced interference effects on buildings—a review of the state-of-the-art. *Engng Struct.* **20**, 617–630.
- KIM, H. J. & DURBIN, P. A. 1988 Investigation of the flow between a pair of circular cylinders in the flopping regime. *J. Fluid Mech.* **196**, 431–448.
- KIM, W., TAMURA, Y. & YOSHIDA, A. 2011 Interference effects on local peak pressures between two buildings. *J. Wind Engng Ind. Aerodyn.* **99**, 584–600.
- KITAGAWA, T. & OHTA, H. 2008 Numerical investigation on flow around circular cylinders in tandem arrangement at a subcritical Reynolds number. *J. Fluids Struct.* **24**, 680–699.
- LIM, H. C., CASTRO, I. P. & HOXEY, R. P. 2007 Bluff bodies in deep turbulent boundary layer: Reynolds number issues. *J. Fluid Mech.* **571**, 97–118.
- LIM, H. C., THOMAS, T. G. & CASTRO, I. P. 2009 Flow around a cube in a turbulent boundary layer: Les and experiment. *J. Wind Engng Ind. Aerodyn.* **97**, 96–109.
- LOZANO-DURAN, A. & JIMENEZ, J. 2014 Effect of the computational domain on direct simulations of turbulent channels up to $Re_\tau = 4200$. *Phys. Fluids* **26**, 011702.

- MARTINUZZI, R. & HAVEL, B. 2000 Turbulent flow around two interfering surface-mounted cubic obstacles in tandem arrangement. *Trans. ASME J. Fluids Engng* **122**, 24–31.
- MASKELL, E. C. 1963 *A Theory of the Blockage Effects on Bluff Bodies and Stalled Wings in a Closed Wind Tunnel*. ARC R&M.
- MERCKER, E., COOPER, K. R., FISCHER, O. & WIEDEMANN, J. 2005 The influence of a horizontal pressure distribution on aerodynamic drag in open and closed wind tunnels. *SAE Trans.* **114**, 921–938.
- NOZAWA, K. & TAMURA, T. 2002 Large eddy simulation of the flow around a low-rise building immersed in a rough-wall turbulent boundary layer. *J. Wind Engng Ind. Aerodyn.* **90**, 1151–1162.
- RICCIARDELLI, F. & VICKERY, B. J. 1998 The aerodynamic characteristics of twin column. *Wind Struct.* **1**, 225–241.
- RICHARDS, P. J., HOXEY, R. P. & SHORT, L. J. 2001 Wind pressure on a 6m cube. *J. Wind Engng Ind. Aerodyn.* **89**, 1553–1564.
- SAKAMOTO, H. & HANIU, H. 1988 Effect of free-stream turbulence on characteristics of fluctuating forces acting on two square prisms in tandem arrangement. *Trans. ASME J. Fluids Engng* **110**, 140–146.
- SALIM, S. M. & CHEAH, S. C. 2009 Wall y^+ strategy for dealing with wall-bounded turbulent flows. In *Proceedings of the International MultiConference of Engineers and Computer Scientists, IMECS 2009, Hong Kong* (ed. S. I. Ao, O. Castillo, C. Douglas, D. D. Feng & J.-A. Lee). Newswood Limited.
- SAUNDERS, J. W. & MELBOURNE, W. H. 1979 Buffeting effects of upstream buildings. In *Proceedings of the Fifth International Conference on Wind Engineering, Fort Collins, Colorado*, pp. 593–606. Pergamon Press.
- SHAH, K. B. & FERZIGER, J. H. 1997 A fluid mechanician's view of wind engineering: large-eddy simulation of flow past a cubical obstacle. *J. Wind Engng Ind. Aerodyn.* **67–68**, 211–224.
- SQUIRES, K. D. 2004 *Detached-Eddy Simulation: Current Status and Perspectives*. Springer.
- SUMNER, D., PRICE, S. J. & PAIDOUSSIS, M. P. 1998 Investigation of side-by-side circular cylinders in steady cross-flow by particle image velocimetry. In *Proceedings 1998 ASME Fluids Engineering, Division Summer Meeting*, vol. 1 (ed. American Society of Mechanical Engineers), p. 37. ASME.
- SUMNER, D., PRICE, S. J. & PAIDOUSSIS, M. P. 1999 Tandem cylinders in impulsively started flow. *J. Fluids Struct.* **13**, 955–965.
- SUMNER, D., RICHARDS, M. D. & AKOSILE, O. O. 2005 Two staggered circular cylinders of equal diameter in cross-flow. *J. Fluids Struct.* **20**, 255–276.
- TANG, U. F. & KWOK, K. C. S. 2004 Interference excitation mechanisms on a 3DOF aeroelastic CAARC building model. *J. Wind Engng Ind. Aerodyn.* **92**, 1299–1314.
- THEPMONGKORN, S., WOOD, G. S. & KWOK, K. C. S. 2002 Interference effects on wind-induced coupled motion of a tall building. *J. Wind Engng Ind. Aerodyn.* **90**, 1807–1815.
- THOOL, K. P., ASHOK, K. A. & ANUPAM, C. 2013 Effect of interference on wind loads on tall buildings. *J. Acad. Indus. Res.* **1** (12), 758–760.
- TIELEMAN, H. W. & AKINS, R. E. 1996 The effect of incident turbulence on the surface pressures of surface-mounted prisms. *J. Fluids Struct.* **10**, 367–393.
- TO, A. P. & LAM, K. M. 2003 Wind-induced interference effects on a group of buildings. In *11th International Conference on Wind Engineering, Texas Tech University, Lubbock, TX*, vol. 1 (ed. D. A. Smith & C. W. Letchford), pp. 2405–2410. IAWE.
- WILLIAMSON, C. H. K. 1985 Evolution of a single wake behind a pair of bluff bodies. *Trans. ASME J. Fluids Engng* **159**, 1–18.
- XIE, Z. T. & CASTRO, I. P. 2008 Efficient generation of inflow conditions for large-eddy simulations of street-scale flows. *J. Flow Turb. Combust.* **81**, 449–470.
- XIE, Z. N. & GU, M. 2004 Mean interference effects among tall building. *Engng Struct.* **26**, 1173–1183.
- XIE, Z. N. & GU, M. 2007 Simplified formulas for evaluation of wind-induced interference effects among three tall building. *J. Wind Engng Ind. Aerodyn.* **95**, 31–52.

- YAKHOT, A., ANOR, T., LIU, H. & NIKITIN, N. 2006 Direct numerical simulation of turbulent flow around a wall-mounted cube: spatio-temporal evolution of large-scale vortices. *J. Fluid Mech.* **566**, 1–9.
- ZDRAVKOVICH, M. M. 1977 Review of flow interference between two circular cylinders in various arrangements. *Trans. ASME J. Fluids Engng* **99**, 618–633.
- ZDRAVKOVICH, M. M. 1987 The effects of interference between circular cylinders in cross flow. *J. Fluids Struct.* **1**, 239–261.
- ZHANG, W. J. & KWOK, K. C. S. 1994 Aeroelastic torsional behaviour of tall buildings in wakes. *J. Wind Engng Ind. Aerodyn.* **51**, 229–248.